*J. Fluid Mech.* (1994), *vol.* 260, *pp.* 351–375



# Evolution of three-dimensional coherent structures in a flat-plate boundary layer

By DIETMAR REMPFER[1] AND HERMANN F. FASEL[2]

[1]Institut für Aerodynamik und Gasdynamik, Universität Stuttgart, 70569 Stuttgart, Germany
[2]Department of Aerospace and Mechanical Engineering, The University of Arizona, Tucson, AZ 85721, USA

(Received 15 December 1992 and in revised form 20 July 1993)

Using a data base generated by a numerical simulation, the three-dimensional coherent structures of a transitional, spatially evolving boundary layer are determined and their spatio-temporal behaviour is investigated in detail. The coherent structures are calculated by the proper orthogonal decomposition method (POD), which leads to an expansion of the flow field variables into Karhunen–Loève eigenfunctions. It is shown that the dynamical coherent structures of the flat-plate boundary layer can be described by pairs of eigenfunctions that contain complete information on the spatial evolution of the structures. It is further demonstrated that first-order coherent structures determined by POD correspond to structures that are observed in experiments. In the region of the boundary layer where the spike signals of transition occur, higher-order coherent structures also play an essential role. By considering these higher-order structures as well as their dynamical behaviour in time, a compact description of the flow phenomena in the boundary layer can be obtained. The description of the events occurring at the spike stages of the transitional boundary layer shows, from a coherent structures point of view, striking similarities to the bursting event of fully turbulent boundary layers.

## 1. Introduction

The last few decades of turbulence research have seen a growing interest in the study of coherent structures of turbulent flows (Robinson 1991). As the philosophy behind the idea of coherent structures is, to a certain extent, the opposite of the philosophy of the statistical theory of turbulence, the coherent structures approach represents a different direction in the investigation of turbulence.

Because instantaneous flow fields are assumed to be hopelessly complex, the classical statistical theory of turbulence (see, for example, Monin & Yaglom 1973) attempts to circumvent this complexity by considering only averaged quantities of the flow variables. While this approach yielded a lot of important results and is probably the one that has contributed the most to our current understanding of the phenomenon of turbulence, it is well known that, with the use of averages, the problem of complexity

simply changes its name to the 'closure problem'. Furthermore, at least from an intuitive point of view, the idea of completely giving up on understanding the details of the motions of a turbulent fluid seems unsatisfactory.

The coherent structures approach to turbulence, on the other hand, relies on a different picture of the turbulence phenomenon. The central idea is that turbulent flows — at least some of them — are not as complex as they appear to be at first sight. Rather, such flows are assumed to be composed of a set of organized motions, each possessing a comparatively simple spatial structure. The apparent complexity of such turbulent flows is then generated by the superposition in space and time of these organized, so-called 'coherent structures'.

The idea of simplicity behind complexity is also a centrepiece of another development that has gained importance within the last few decades, namely the study of nonlinear dynamical systems. It has been shown that very simple systems of ordinary differential equations (ODE's) possessing as few as three degrees of freedom can give rise to extremely complex, 'chaotic' behaviour (Lorenz 1963). In connection with the success of dynamical systems theory, it seemed natural to look at turbulence as a chaotic phenomenon in the sense of the theory of ordinary differential equations. In trying to use dynamical systems theory — particularly for the case of open flow systems like the flat-plate boundary layer considered in this paper — one is confronted with the question of what kind of modes of the flow are going to be described by the ODE's.

This is exactly the issue where the concept of coherent structures becomes additionally relevant: if a turbulent flow could be considered as being composed of the superposition of a possibly small number of coherent structures, the equations describing the evolution of such structures are candidates for a low-dimensional description of turbulence.

The considerations given above motivated the work (Rempfer 1991) upon which the present paper is based. Using data from a highly resolved numerical simulation (Rist, Kloker & Fasel 1994), the evolution and dynamical behaviour of the coherent structures in a flat-plate boundary layer were investigated in detail. In addition, by Galerkin projection of the Navier–Stokes equations onto a system of empirical eigenfunctions (similar to the work of Zhou & Sirovich 1992, see also Aubry *et al.* 1988), a system of ordinary differential equations has been derived that describes the evolution of the coherent structures. Within the region where the boundary layer has started to get turbulent, this system of ODE's indeed displayed low-dimensional deterministic chaos. In order to keep the present paper at a reasonable length, these parts of the investigation are reported elsewhere (Rempfer 1991, 1993). Here, we focus on our results concerning the evolution of coherent structures in the transitional regime.

The domain considered (see § 2) contains the stages of the transition process from the initial three-dimensional, nonlinear development of Tollmien–Schlichting waves up to just beyond the spike stages. The coherent structures within this region were determined using the method of *proper orthogonal decomposition* (POD). This method was first used in 1967 by Bakewell & Lumley (1967) for the calculation of near-wall coherent structures. With the advent and general availability of powerful computers, roughly since the beginning of the 1980s, this method has been applied to an increasing number of flows. For example, Glauser & George (1987), Kirby, Boris & Sirovich (1990) and Sirovich, Kirby & Winter (1990) used POD to identify coherent structures in axisymmetric jets, and Glezer, Kadioglu & Pearlstein (1989), Delville, Bellin & Bonnet (1990) and Rajaee & Karlsson (1990) investigated two-dimensional

structures of free shear layers. Proper orthogonal decomposition was employed by Moin & Moser (1989), Sirovich, Ball & Keefe (1990) and Ball, Sirovich & Keefe (1991) to calculate coherent structures in channel flows. The work by Moin & Moser was the first to identify three-dimensional coherent structures; however, in contrast to our work they were forced to apply a so-called *shot-noise decomposition* (Lumley 1970) for the homogeneous directions of their flow.

From experimental (see, for example, Hama & Nutant 1963; Williams, Fasel & Hama 1984; Perry, Lim & Teh 1981) and numerical (Kleiser & Zang 1991; Rist *et al.* 1994) evidence, it is quite clear that coherent structures exist for transitional boundary layers. The motivation for applying POD to a transitional flat-plate boundary layer was twofold. First, it was by no means clear that POD would be able to extract the dynamical coherent structures of a spatially evolving flow like the one we were investigating. Sirovich (1989) raised serious doubts as to the suitability of POD for representing coherent structures with respect to the intuitive meaning of this term and stressed that '*the relation between the eigenfunctions of the POD and coherent structures is unclear*' (p. 140; emphasis is ours). Furthermore, to our knowledge, the method of POD has never been used to extract fully three-dimensional eigenfunctions from spatial simulations (or experiments) of open flow systems (there exists, however, such an application of POD to Rayleigh–Bénard convection in a closed box, see Sirovich & Park 1990; Park & Sirovich 1990). In all cases where three-dimensional coherent structures of open flows have been identified using POD, the assumption of streamwise periodicity of the flow was made. In contrast, in the simulation of Rist *et al.* (1994), the flow shows a distinct evolution in the streamwise direction eventually leading to laminar–turbulent transition. Therefore, as a first objective we want to demonstrate that POD is indeed a suitable tool for determining spatially developing coherent structures. Because of its relative simplicity, the transitional boundary layer is an ideal test case for this purpose.

Second, the notion of a 'coherent structure' is of little use as long as it is not possible to give a precise description of the role that these structures play in the dynamics of complex transient flows. In order to be able to give such a description, we need an exact mathematical definition of the flow fields corresponding to the coherent structures. While it is true that at least the most energetic structures we found by applying POD could have been found as well just by inspection, such a decomposition of the flow phenomena based on intuition is generally not accessible to a mathematical treatment. In comparison, proceeding from a mathematical description of the coherent structures as yielded by the POD, it is possible to directly derive an energy equation for the coherent structures from the Navier–Stokes equations. By investigating this energy equation, we then can explore the mechanisms behind the dynamical behaviour of the coherent structures and their contribution to the dynamics of the flow as a whole. This part of our work will be reported in a subsequent paper (Rempfer & Fasel 1994).

The numerical simulation that produced the data base for the calculation of the empirical eigenfunctions is briefly described in § 2. As the POD method is now widely known, only a short outline of the method, focusing on some of the properties of the formalism that are relevant to this investigation, is given in § 3. A description of the evolution of the coherent structures in a transitional boundary layer based on the behaviour of the most energetic structures of the flow is given in § 4, and § 5 presents a closer look at the higher-order structures in a region of the boundary layer where the spike signals of transition occur. Some conclusions are drawn in § 6 together with a discussion on future work.

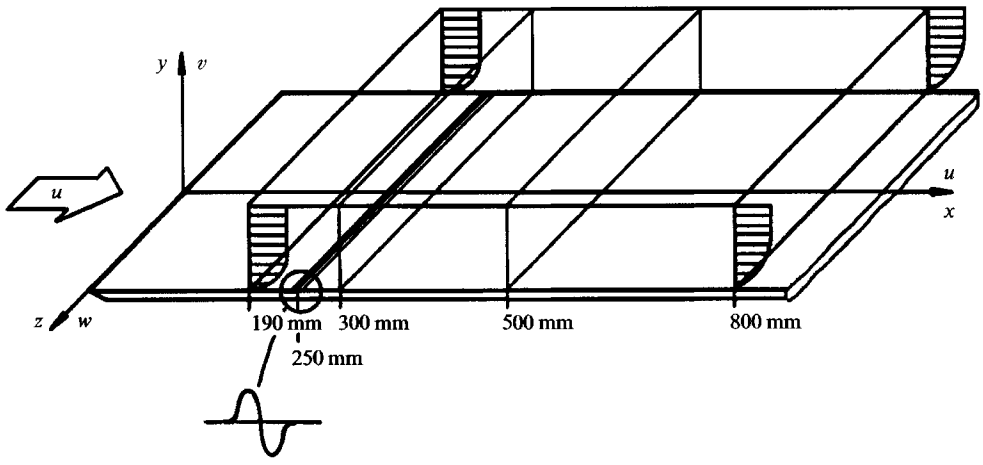


FIGURE 1. Integration domain of numerical simulation by Rist et al. (1994).

## 2. Numerical simulation

To calculate the three-dimensional structures of a flow, the POD requires a data base of spatially highly resolved flow fields at a number of time steps large enough so that the statistical averages in time are meaningful. At this time, such a data base can only be generated by numerical simulations. For our investigations, we were able to use the data from a numerical simulation by Rist *et al.* (1994), who simulated a wind tunnel experiment by Kachanov *et al.* (1985) on controlled transition in a flat-plate boundary layer. In their work, Rist *et al.* performed a direct Navier–Stokes simulation of the spatial development of an incompressible flow. The integration domain that was used and the corresponding coordinate system are shown in figure 1. As shown in this figure, the symbols $x$, $y$, and $z$ were used for the streamwise, wall-normal and spanwise coordinates, respectively, and $u$, $v$, and $w$ were used for the corresponding velocity components. For the simulation, a numerical method was developed employing finite difference approximations for the $x$- and $y$-coordinates while the spanwise coordinate was discretized in function space using Fourier modes. The discretization used for the integration domain shown in figure 1 consisted of $4000 \times 120$ nodes for the streamwise and wall-normal directions, respectively, and included 16 Fourier harmonics for the spanwise direction. To simulate the experiment on controlled transition by Kachanov *et al.*, Rist *et al.* introduced regular disturbances via their boundary condition for the wall-normal ($v$-) velocity component. As in the experiment, these disturbances were periodic in time and symmetric with respect to selected $(x, y)$-planes (the peak or valley planes). It is important to note that, as the Navier–Stokes equations preserve such symmetries, Rist *et al.* were able to assume, without loss of generality, symmetry of their flow fields with respect to the $(x, y)$-plane. This property is of special importance when using POD for the calculation of coherent structures (see the discussion in the following section).

From the data generated by the simulation described above, we used the values of the velocity vector within a certain three-dimensional window of the computational domain. The region investigated corresponds to a rectangular box 8.77 mm high and 24.5 mm wide in the spanwise direction. In the streamwise direction the box extends from $x = 300$ mm to $x = 500$ mm, with $x$ denoting the distance from the flat-plate leading edge. With a free-stream velocity of 9.09 m/s, the Reynolds number based

on momentum thickness was $Re_{\delta_2} = 283$ at the inflow and $Re_{\delta_2} = 575$ at the outflow boundary of the domain. Thus, the region considered here is composed of the stages of the transition process from the initial three-dimensional, nonlinear development of Tollmien-Schlichting waves up to just beyond the spike stages. Within the first 70% of the downstream extent of this region, the time behaviour of the flow is almost exactly periodic, but slight deviations from periodicity, indicating the onset of turbulence, can be observed within the last quarter of the domain. The ensemble of flow fields used in this work consisted of 440 equally spaced time steps within one time period of the prescribed disturbances. These flow fields were discretized on a $695 \times 110$-grid for the $x$- and $y$-directions and included 16 Fourier harmonics for the spanwise ($z$-) direction.

## 3. The proper orthogonal decomposition

Lumley (1967) was the first to suggest the use of the Karhunen–Loève procedure of probability theory (Loève 1955) to identify the coherent structures of random turbulent flows. This method, which is now widely known as proper orthogonal decomposition (POD), has the advantage that an ensemble of flow fields is the only information required to obtain the coherent structures of a flow. Thus, there is no need for external information, any prior knowledge, or even an understanding of the flow. This method is discussed briefly below, along with some of its properties that are of particular importance for our problem.

We start by pointing out the special properties of the flow fields being investigated. It may be noted parenthetically that these are not necessary restrictions, and that the POD can be applied under more general conditions as well (see Lumley 1970). As we will confine ourselves to finite regions in space, all the functions appearing in the formulae below can be viewed as being of finite support and hence, on physical grounds, being square integrable. Thus, the integrals used below are defined in the ordinary Riemannian sense, the integration domain $D$ being a finite region in space. Therefore, the flow fields we are investigating belong to the Hilbert space of real, square-integrable functions, where a scalar product can be defined by

$$(\boldsymbol{a}, \boldsymbol{b}) = \int_D \boldsymbol{a}(\boldsymbol{x}) \cdot \boldsymbol{b}(\boldsymbol{x}) \, \mathrm{d}\boldsymbol{x}, \tag{3.1}$$

and a suitable norm is

$$\|\boldsymbol{a}\| = (\boldsymbol{a}, \boldsymbol{a})^{\frac{1}{2}}. \tag{3.2}$$

In our evaluation of averages we make use of the ergodic hypothesis by substituting time averages for the ensemble averages denoted by $\langle \cdot \rangle$, which is clearly justified for the almost time-periodic processes being considered. These time averages are ordinary arithmetic mean values for realizations $\boldsymbol{u}^{\ell}(\boldsymbol{x}) = \boldsymbol{u}(\boldsymbol{x}, t_{\ell})$ that are equally spaced in time.

Now, a characteristic structure $\boldsymbol{\sigma}(\boldsymbol{x})$ may be defined by the property that its flow field is, in some average sense, as similar as possible to the flow realizations $\boldsymbol{u}^{\ell}(\boldsymbol{x})$ of the velocity fields of the given ensemble. This can be expressed mathematically as

$$\frac{\langle (\boldsymbol{u}^{\ell}, \boldsymbol{\sigma})^2 \rangle}{\|\boldsymbol{\sigma}\|^2} \stackrel{!}{=} \text{Max.}, \tag{3.3}$$

which means that we specify the structure $\boldsymbol{\sigma}$ by requiring that its projection on the flow realizations shall be maximum in quadratic mean. Using the calculus of variations,

the problem can be reduced to the Fredholm integral equation

$$\int_D \boldsymbol{R}(x,x')\cdot\boldsymbol{\sigma}(x')\,\mathrm{d}x' = \lambda\boldsymbol{\sigma}(x) \tag{3.4}$$

representing an eigenvalue problem for the structure $\boldsymbol{\sigma}$ (see Lumley 1970 for details of the derivation). The kernel $\boldsymbol{R}$ of this equation is the autocorrelation function

$$\boldsymbol{R}(x,x') = \langle \boldsymbol{u}(x)\boldsymbol{u}(x')\rangle, \tag{3.5}$$

where the term inside the brackets denotes a dyadic product. Because this kernel has the form of a symmetric, non-negative definite Hilbert–Schmidt operator, there exists a denumerable infinite set of real solutions $\boldsymbol{\sigma}_j$ and corresponding eigenvalues $\lambda_j$.

For the case of three-dimensional flow fields $\boldsymbol{u}^\ell$, the eigenvalue problem (3.4) soon becomes intractable even at only moderate spatial resolution. It is therefore beneficial to transform (3.4) by expressing $\boldsymbol{\sigma}$ as a linear combination of the instantaneous flow fields

$$\boldsymbol{\sigma} = \sum_{\ell=1}^{M} q_\ell \boldsymbol{u}^\ell, \tag{3.6}$$

where $M$ is the number of realizations given. By introducing this ansatz together with the expression for the autocorrelation tensor,

$$\boldsymbol{R}(x,x') = \frac{1}{M}\sum_{\ell=1}^{M} \boldsymbol{u}^\ell(x)\boldsymbol{u}^\ell(x'), \tag{3.7}$$

into (3.4), we get the algebraic eigenvalue problem

$$\boldsymbol{C}\boldsymbol{q} = \lambda\boldsymbol{q}, \tag{3.8}$$

where

$$C_{jk} = \frac{1}{M}(\boldsymbol{u}^j,\boldsymbol{u}^k). \tag{3.9}$$

In this representation, the order of the eigenvalue problem only depends on the number, $M$, of realizations given and is unaffected by spatial resolution. Therefore this method, referred to by Sirovich (1987) as the *method of strobes*, is used to calculate the eigenfunctions.

Before proceeding with the properties of the solutions of (3.4) (or (3.8)) some remarks on the problem of homogeneous directions are in order. Within our context, by the concept of 'homogeneous direction' we denote a coordinate, say $z$, where the correlation function becomes translationally invariant so that it can be written

$$\boldsymbol{R}(x,x',y,y',z,z') = \boldsymbol{R}(x,x',y,y',z-z'). \tag{3.10}$$

It can then be shown that the eigenfunctions $\boldsymbol{\sigma}$ can be expressed as

$$\boldsymbol{\sigma}(x) = \boldsymbol{\varphi}(x,y;k)\mathrm{e}^{\mathrm{i}2\pi kz/L}, \quad k = 0,1,2,\ldots, \tag{3.11}$$

where it was additionally assumed that the flow fields are not only homogeneous, but also periodic in the $z$-direction with a periodicity length of $L$, an assumption that is frequently made in numerical simulations. If periodicity is dropped, the spectrum of the eigenvalues of (3.4) becomes continuous and the proper orthogonal decomposition degenerates to a Fourier transform in the homogeneous direction. Now, the problem with the eigenfunctions in (3.11) is that they are products of some function in $x$ and $y$ and a simple sinusoid in the $z$-direction. Such a form of a

'coherent structure' contradicts intuition as well as experimental observations, where coherent structures are found to be compact in space, while a sinusoid is certainly not a compact function. This situation lead some researchers to believe that the POD would not be able to extract the coherent structures of flows possessing homogeneous directions. Additional techniques, like 'shot-noise decomposition' (Lumley 1970; Moin & Moser 1989) have sometimes been used to overcome this problem and to assemble a coherent structure (or a 'characteristic eddy' in the case of Moin & Moser 1989) that is compact in the homogeneous direction as well. Such procedures, however, are questionable because they reintroduce — although on a more subtle level — the need to predict properties of the coherent structure before it is actually known.

The reason we did not have to deal with this kind of problem is due to the symmetry of the flow fields calculated in the numerical simulation from which we took our data. Because our flow fields are symmetric with respect to the $(x, y)$-plane, the functions we are investigating are not homogeneous in the spanwise direction and the homogeneous translation group does not apply. Imaginatively speaking, this means that we have set up our flow in such a way that the coherent structures align along the $x$-axis rather than occurring at arbitrary positions in the spanwise direction. Therefore the eigenfunctions of the POD cannot be factorized as in (3.11) and, instead, truly reproduce the coherent structures of our flow, as will be shown in the next section. Before turning to the results, we will restate some of the properties of the Karhunen–Loève eigenfunctions of the POD.

(*a*) The different eigenfunctions are orthogonal and can be normalized arbitrarily. We chose to normalize the coherent structures according to

$$(\boldsymbol{\sigma}_j, \boldsymbol{\sigma}_k) = \lambda_j \delta_{jk}. \tag{3.12}$$

The justification for this choice is discussed below in connection with equation (3.15).

(*b*) The set of the eigenfunctions $\boldsymbol{\sigma}_j$ is complete in the sense that the flow fields of the ensemble given can be expanded in the eigenfunctions via

$$\boldsymbol{u}(\boldsymbol{x}, t_\ell) = \sum_j \zeta_j(t_\ell) \boldsymbol{\sigma}_j(\boldsymbol{x}), \tag{3.13}$$

where

$$\zeta_j(t_\ell) = \frac{(\boldsymbol{u}', \boldsymbol{\sigma}_j)}{\lambda_j}. \tag{3.14}$$

We note that, instead of using (3.14), the expansion coefficients $\zeta_j$ could also be calculated directly from an eigenvalue problem that is completely analogous to (3.4). This eigenvalue problem can be obtained by exchanging time and space in (3.4) and (3.5) (Sirovich 1987, see also Aubry, Guyonnet & Lima 1991, where the resulting temporal eigenfunctions — the expansion coefficients $\zeta_j(t)$ in our terminology — are called *chronoi* and our spatial eigenfunctions $\boldsymbol{\sigma}_j(\boldsymbol{x})$ are termed *topoi*).

(*c*) The expansion coefficients are uncorrelated in time, and, with the normalization (3.12), we have

$$\langle \zeta_j \zeta_k \rangle = \delta_{jk}. \tag{3.15}$$

Thus, the eigenfunctions $\boldsymbol{\sigma}_j$, after being normalized according to (3.12), represent the root-mean-square values of the flow fields that are induced by the corresponding structure.

(*d*) We define the energy of a flow field as

$$e = \frac{1}{2}\int_D \boldsymbol{u}^2(\boldsymbol{x})\,\mathrm{d}\boldsymbol{x}. \tag{3.16}$$

Introducing (3.13) into (3.16), we find, for the time average of the energy,

$$\langle e\rangle = \frac{1}{2}\sum_j \lambda_j. \tag{3.17}$$

The eigenvalues of (3.4) are therefore all non-negative, and they represent the mean value of the energy that the corresponding coherent structure contributes to the flow. In that sense the eigenvalues $\lambda_j$ are a measure of the related structure's importance to the flow. In § 5, however, we will discuss a certain pair of eigenfunctions that, despite its low eigenvalues and corresponding low average energy, strongly influences the dynamics of the flow.

By comparing (3.13) and (3.3), one of the most significant properties of the system of Karhunen–Loève eigenfunctions can be seen immediately. It becomes obvious that the eigenfunctions have been defined in such a way that the convergence of a representation of the flow field is optimally fast in the mean square. This means that of all possible systems of eigenfunctions, the one described by (3.3) needs the smallest number of terms to represent the flow fields to a given accuracy. This property is clearly attractive if one is interested in a low-dimensional description of a turbulent flow via a system of ordinary differential equations. Once one has decided that time should be the independent variable of this system of ODE's, which — although not being mandatory — seems to be a natural choice, the POD delivers an optimum system of eigenfunctions for such a description. Finally, we point out that, as the coherent structures can be represented as linear combinations of the given flow fields, these eigenfunctions inherit all those properties of the instantaneous flow fields that can be expressed in the form of linear homogeneous equations.

## 4. Coherent structures of transition: phenomenology

We start by looking at some of the special properties of the POD eigenfunctions representing the coherent structures in the case of transition in an incompressible, spatially evolving boundary layer. Because the eigenfunctions are linear combinations of instantaneous flow fields, as was mentioned above, it can be concluded that each of the eigenfunctions forms a solenoidal vector field representing a kinematically possible velocity field of an incompressible flow. Furthermore, each of the boundary conditions of the flow as a whole is satisfied by any eigenfunction individually. Thus, for example, the no-slip condition at the wall is met by each eigenfunction.

Now, if one intends to find the coherent structures of a spatially evolving flow, a fundamental problem arises at first sight. This is due to the fact that, if coherent structures exist in such a flow, one has to expect that they are not only carried downstream but that, in general, they will be deformed as they propagate. The eigenfunctions of the POD, on the other hand, represent flow fields with stationary streamlines, so the question arises as to how these eigenfunctions could capture the situation in a spatially evolving flow.

To answer this question, the eigenvalues of decompositions of the flow fields in the regions $D_1$, $D_2$, and $D_3$ (described in table 2) are shown in table 1. As mentioned above, these eigenvalues represent two times the average energy that the corresponding

| | $\lambda_j$ | | |
|---|---|---|---|
| $i$ | $D_1$ | $D_2$ | $D_3$ |
| 1 | $9.80 \times 10^{-4}$ | $9.54 \times 10^{-4}$ | $9.31 \times 10^{-4}$ |
| 2 | $1.15 \times 10^{-7}$ | $4.08 \times 10^{-7}$ | $7.63 \times 10^{-7}$ |
| 3 | $1.12 \times 10^{-7}$ | $3.93 \times 10^{-7}$ | $7.40 \times 10^{-7}$ |
| 4 | $5.28 \times 10^{-8}$ | $4.50 \times 10^{-8}$ | $1.48 \times 10^{-7}$ |
| 5 | $5.21 \times 10^{-8}$ | $4.40 \times 10^{-8}$ | $1.43 \times 10^{-7}$ |
| 6 | $1.90 \times 10^{-8}$ | $8.16 \times 10^{-9}$ | $7.04 \times 10^{-8}$ |
| 7 | $1.89 \times 10^{-8}$ | $7.96 \times 10^{-9}$ | $6.81 \times 10^{-8}$ |
| 8 | $1.03 \times 10^{-9}$ | $4.37 \times 10^{-9}$ | $6.60 \times 10^{-8}$ |
| 9 | $1.03 \times 10^{-9}$ | $4.17 \times 10^{-9}$ | $6.49 \times 10^{-8}$ |
| $\sum_{j=2}^{\infty} \lambda_j$ | $2.38 \times 10^{-7}$ | $9.29 \times 10^{-7}$ | $2.83 \cdot 10^{-6}$ |

TABLE 1. Eigenvalues of POD for regions $D_1$, $D_2$, and $D_3$.

eigenfunction contributes to the flow. The noise floor of the numerical simulation that produced our data is of the order of $10^{-7}$–$10^{-6}$. Therefore, we can expect our POD eigenfunctions to represent structures of the flow (as opposed to structures of the numerical noise) up to a range of eigenvalues of at least 12 orders of magnitude. All the structures being discussed in this paper are well above this limit.

The first eigenfunction of the POD, corresponding to the first eigenvalue in table 1, is almost identical with the mean flow $\bar{\boldsymbol{u}} = \langle \boldsymbol{u} \rangle$. For instance, plots of $y$-profiles of the $u$-velocity components corresponding to $\bar{\boldsymbol{u}}$ and $\boldsymbol{\sigma}_1$ are virtually indistinguishable. This eigenfunction therefore should not be referred to as a coherent structure in the usual sense. The second and higher eigenvalues, however, belong to the actual coherent structures of the flow. What is notable about these eigenvalues is that they occur in pairs of almost equal value, whereas there is a large gap in magnitude between them. This pattern is identical to the one that Rajaee, Karlsson & Sirovich (1992) found in their work. The reason for this behaviour can be understood when we look at figure 2, where contour lines of the $u$-velocity component of the first pair of eigenfunctions, $\boldsymbol{\sigma}_2$ and $\boldsymbol{\sigma}_3$, and the time behaviour of the corresponding expansion coefficients are shown. It can be seen that, essentially, the eigenfunctions of this pair are representing the same structure, one of them just being shifted with respect to the other in the streamwise direction. Figure 2 (*c*) shows that the corresponding expansion coefficients, $\zeta_2$ and $\zeta_3$, are analogously phase-shifted in time. Thus, if we multiply each of the eigenfunctions of such a pair by its corresponding expansion coefficient, we get a structure that is moving in the streamwise direction. Most of the structures we found propagate at a velocity between 40% and 50% of the free-stream velocity. Within our regions $D_1$ and $D_2$ this velocity is approximately (within 10% accuracy) equal to the mean-flow velocity at the level in $y$ where the highest Reynolds stress occurs. This result is in agreement with findings of Sirovich *et al.* (1990, 1991). We can therefore conclude that the dynamical coherent structures, $\varsigma_j(x,t)$, of our spatially evolving flow are represented by pairs of eigenfunctions according to

$$\varsigma_j(x,t) = \zeta_{2j}(t)\boldsymbol{\sigma}_{2j}(x) + \zeta_{2j+1}(t)\boldsymbol{\sigma}_{2j+1}(x). \tag{4.1}$$

In this paper we will refer to $\varsigma_j$ as representing the 'coherent structure of order $j$' (or '$j$th-order coherent structure'). The eigenfunction $\boldsymbol{\sigma}_1$ represents the 'coherent structure of order 0'. A pair of eigenfunctions, $\boldsymbol{\sigma}_{2j}$ and $\boldsymbol{\sigma}_{2j+1}$, not only contains

| $D_1$ | $D_2$ | $D_3$ |
|---|---|---|
| $300\,\text{mm} \leqslant x \leqslant 369\,\text{mm}$ | $369\,\text{mm} \leqslant x \leqslant 438\,\text{mm}$ | $431\,\text{mm} \leqslant x \leqslant 500\,\text{mm}$ |
| $182000 \leqslant \text{Re}_x \leqslant 224000$ | $224000 \leqslant \text{Re}_x \leqslant 265000$ | $261000 \leqslant \text{Re}_x \leqslant 303000$ |
| $284 \leqslant \text{Re}_{\delta_2} \leqslant 316$ | $316 \leqslant \text{Re}_{\delta_2} \leqslant 430$ | $408 \leqslant \text{Re}_{\delta_2} \leqslant 575$ |
| | $0.00\,\text{mm} \leqslant y \leqslant 8.77\,\text{mm}$ | |
| $y_{\max} \approx 3.1\delta$ | $y_{\max} \approx 2.8\delta$ | $y_{\max} \approx 2.2\delta$ |
| | $-12.25\,\text{mm} \leqslant z \leqslant 12.25\,\text{mm}$ | |

TABLE 2. Basic parameters of investigated regions. $Re_{\delta_2}$ denotes the Reynolds number formed with the momentum thickness $\delta_2$, $Re_x$ is the Reynolds number based on the $x$-position.

complete information on the typical shape of the corresponding coherent structure, but also shows the evolution that the coherent structure undergoes while moving downstream. Also, it is clear from (4.1) that each of the eigenfunctions of a pair represents the coherent structure at a certain instant in time, namely the one when the expansion coefficient of the other eigenfunction vanishes. We would like to point out that the representation (4.1) of the dynamical coherent structures of our flow forms the basis for a discussion of the dynamical behaviour and the evolution of coherent structures.

In (Aubry, Guyonnet & Lima 1992) it is shown that the near-degeneracy of the eigenvalue problem (3.4) is a consequence of the spatio-temporal symmetries being connected with the presence of travelling waves (or structures) in our flow. We note that the eigenvalues corresponding to a pair of eigenfunctions are not exactly the same, as a consequence of the spatial evolution of the boundary layer and, accordingly, of the changes that the structures undergo. For the case of a parallel flow where structures of constant shape are travelling downstream at constant speed, the problem (3.4) would be degenerate, yielding pairs of identical eigenvalues.

We will now illustrate the evolution of coherent structures during transition by first presenting only the most energetic structure represented by the first pair of eigenfunctions. In figures 4–6, we show these structures in three consecutive downstream regions of the boundary layer. The basic parameters for these regions are summarized in table 2. The length of the regions corresponds to approximately two Tollmien–Schlichting wavelengths, and it was chosen such that two specimens of each structure can be observed in each of the figures. The structures are represented by isosurfaces of the $u$- and $v$-velocity components of the $\varsigma_1$. The corresponding eigenfunctions have been determined by applying the POD separately to the regions $D_1$, $D_2$, and $D_3$. As the structures move to the right (downstream) with the flow (note that this flow is, to a good approximation at least, time-periodic), the second (downstream) structure can be regarded as a later stage in the evolution of a coherent structure that before had the shape of the one to the left. Each of the structures is shown at the instant in time when the shape of both specimens can be discerned most clearly. For example, from figure 4, where the first-order structures of region $D_1$ are shown, we can observe how the isosurface of the $u$-velocity component resembling a flat tube develops a delta-shaped ledge at its upper side (figure 4*a*). The $v$-velocity isosurface (figure 4*b*) resembles a tube that is being bent along the spanwise axis. The corresponding structures for the next downstream region are shown in figure 5. It can be observed how the surface of the $u$-velocity component, which on the left has assumed an arrowhead-like form, evolves into the shape of the well-known $\Lambda$-vortex

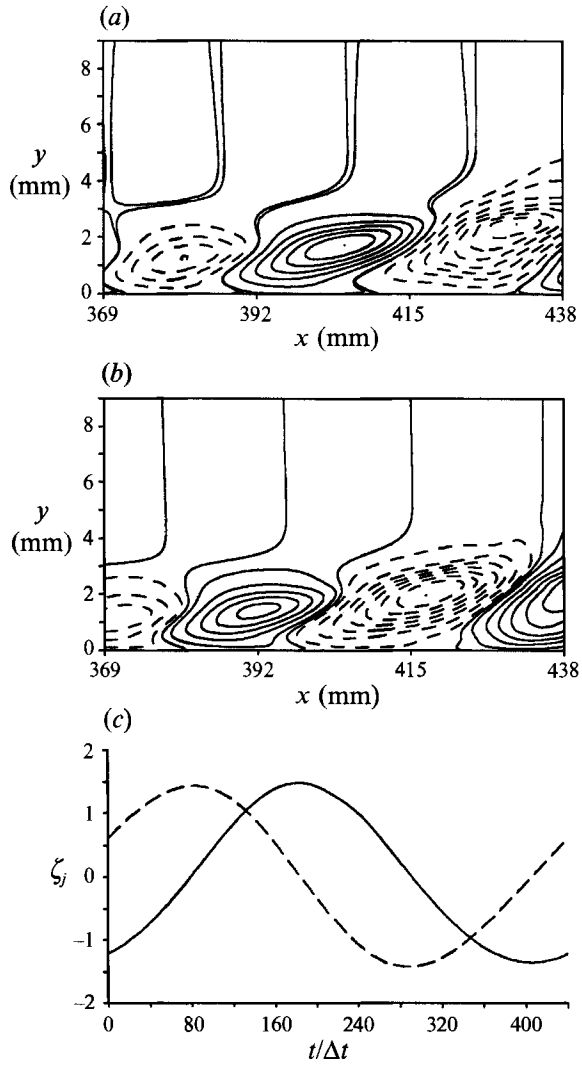


FIGURE 2. Contour lines of $u$-velocity component of the pair of eigenfunctions $\sigma_{2/3}$ between $x = 369$ mm and $x = 438$ mm (region $D_2$) in the plane $z = 0$ (peak plane) and time behaviour of the corresponding expansion coefficients.

(figure 5*a*). The former tube-like structure of the $v$-velocity surface (figure 4*b*) has already split up into two parts. Finally, in figure 6, which shows the evolution in region $D_3$, the former $\Lambda$-vortex is being highly stretched in the streamwise direction and the $u$-velocity surface and that of the $v$-velocity component develop into much more complex shapes.

Figures 4–6 also show an increasing degree of 'three-dimensionality' of the structures. This evolution can be quantified by computing the energies of the different spanwise harmonics for the velocity fields $\varsigma_1$. Such a calculation shows that for the first-order structure in our region $D_1$ (this structure approximately represents a two-dimensional Tollmien–Schlichting wave, see below), about 94% of the energy of this structure is contained in the two-dimensional component (the zeroth spanwise

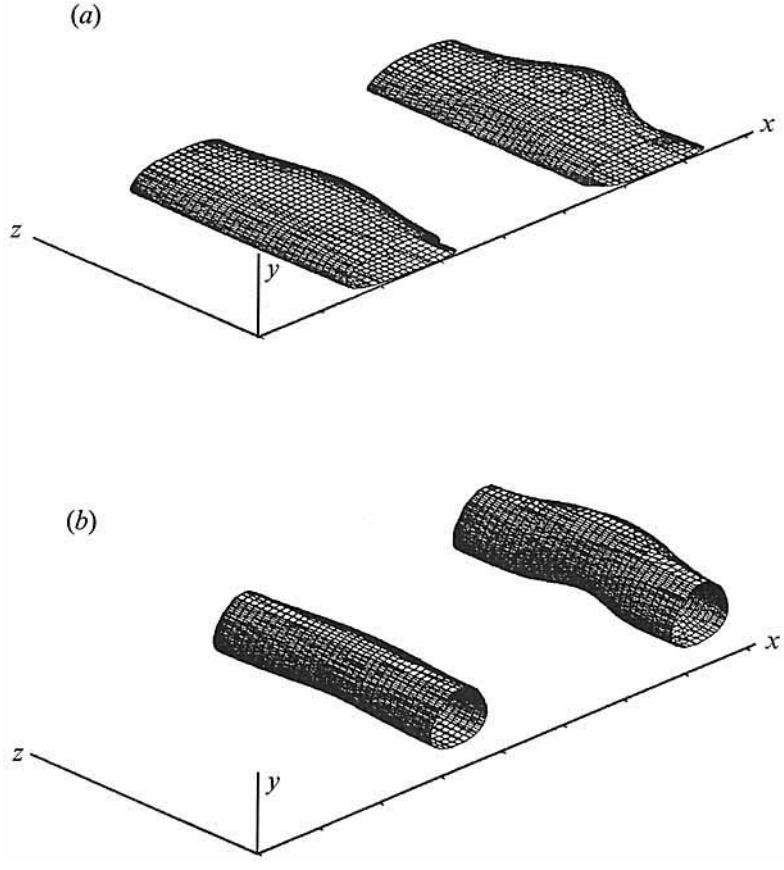


FIGURE 3. Contour surfaces of coherent structure of first order in region $D_1$, $\Lambda_1^c \approx 0.95$, $t/\Delta t = 170$ (300 mm $\leqslant x \leqslant$ 369 mm).

harmonic). In region $D_2$, however, this proportion has dropped to about 30%, and in region $D_3$ only 14.5% of the energy is contained in the two-dimensional component.

The rising spatial complexity of the flow field can also be inferred from the decrease of the contribution $\Lambda_1^c$ of the first-order structure to the energy of the fluctuating flow. This contribution can be calculated from

$$\Lambda_j^c = \frac{\frac{1}{2}(\lambda_{2j} + \lambda_{2j+1})}{\left\langle \frac{1}{2}\int_D \boldsymbol{u}'^2(\boldsymbol{x})\,\mathrm{d}\boldsymbol{x} \right\rangle} = \frac{\lambda_{2j} + \lambda_{2j+1}}{\sum_{j=2}^{\infty}\lambda_k}. \tag{4.2}$$

This contribution decreases from 95% in the first region, to 86% in the second, to 53% in the last region investigated. The decline of these relative energies is because additional coherent structures, generated as the structures move downstream, take their share from the total energy available. As a consequence, from the POD point of view, more and more eigenfunctions are needed to adequately represent the spatial complexity of the different flow fields that are found in the given ensemble.

In figure 6, the $u$-velocity surface of the coherent structure from figure 5 is compared to a photograph of a visualization of the $\Lambda$-vortex using time lines (Hama & Nutant

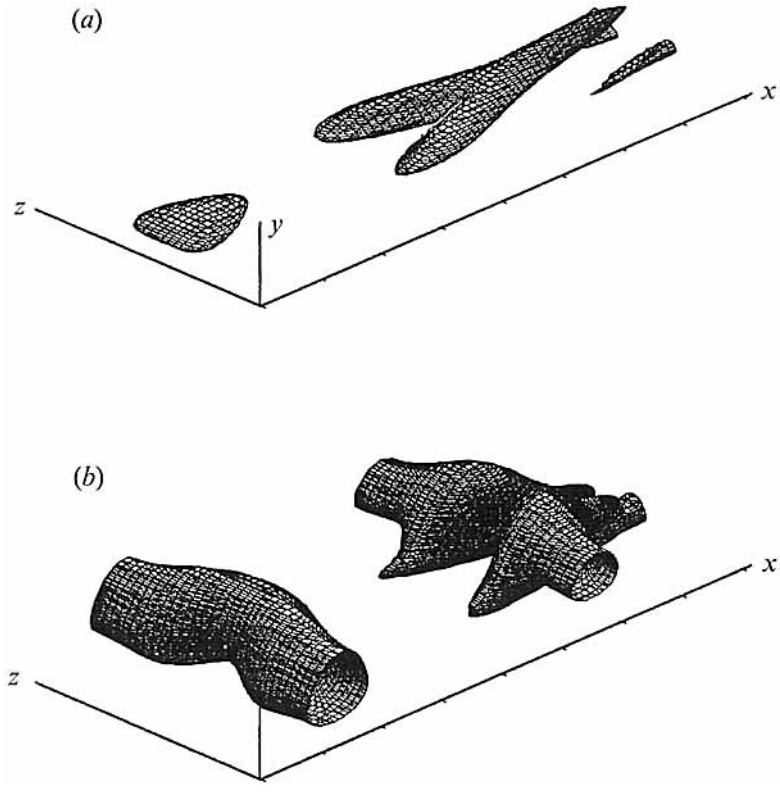


FIGURE 4. Contour surfaces of coherent structure of first order in region $D_2$, $\Lambda_1^c \approx 0.86$, $t/\Delta t = 350$ (369 mm $\leqslant x \leqslant$ 438 mm).

1963). Although the isosurface for the $u$-velocity of the coherent structure shown is not directly comparable to the time lines of the experiment, figure 6 still demonstrates a good qualitative similarity between the corresponding flow fields. Thus, we can give an affirmative answer to the question raised in the beginning, namely, is POD suited for the identification of coherent structures. What we have found is that POD is capable of identifying coherent structures that are similar to those found in an intuitive fashion.

Based on the plots shown in figure 7, we can also comment on connections between the Karhunen–Loève eigenfunctions of the POD and the Orr–Sommerfeld eigenfunctions of linear stability theory. In figure 7, $u$-velocity profiles of two-dimensional Tollmien–Schlichting waves (i.e. linear waves that are travelling in the streamwise direction) are compared to the corresponding rms-values of the two-dimensional $u$-velocity component (zeroth spanwise harmonic) being induced by the first order structure $\varsigma_1$. Both profiles have been normalized such that the maximum amplitude is equal to one. Figure 7 shows that at the very beginning of our domain ($x$ = 300 mm), the two profiles are indeed almost identical. As the flow at that position is close to a linear superposition of a steady, two-dimensional Blasius boundary layer and a low-amplitude Tollmien–Schlichting wave, this result could be expected intuitively. In fact, it has been shown by Breuer & Sirovich (1991) that the Karhunen–Loève analysis, when applied to the linearized problem, exactly reproduces

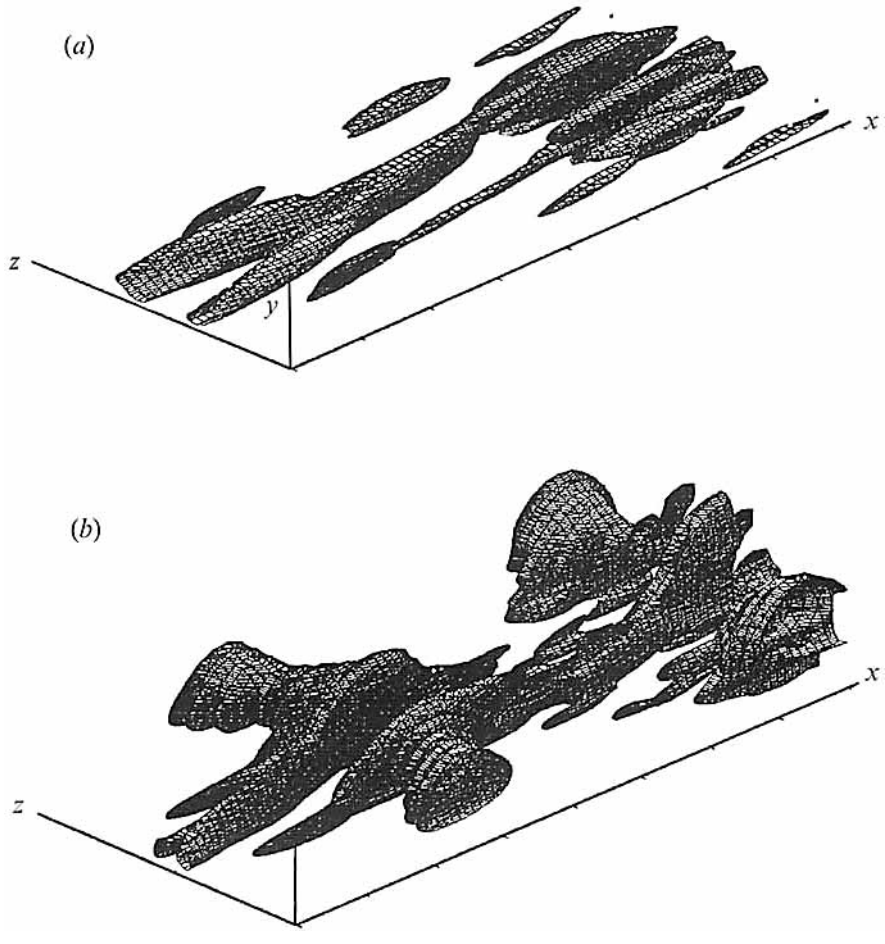


FIGURE 5. Contour surfaces of coherent structure of first order in region $D_3$, $\Lambda_1^c \approx 0.53$, $t/\Delta t = 300$ (431 mm $\leqslant x \leqslant$ 500 mm).

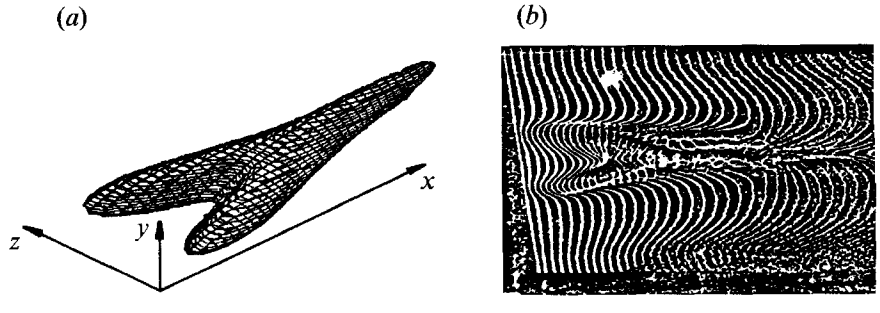


FIGURE 6. Comparison of coherent structure of first order in $D_2$ to experimental visualization of $\Lambda$-vortex.

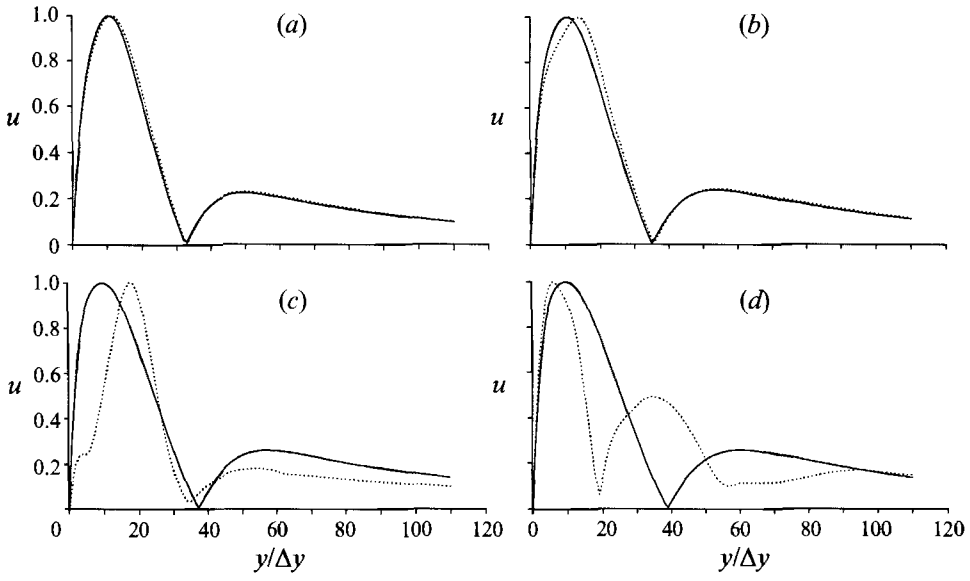


FIGURE 7. Comparison of $u$-velocity profiles of Karhunen–Loève eigenfunctions and Orr–Sommerfeld eigenfunctions. ————, OS eigenfunction; ·····, rms-profile of coherent structure $\varsigma_1$.

the eigenfunctions of linear theory. From figures 7 (*b*) and 7(*c*) it can be seen, however, that, at positions further downstream, the corresponding eigenfunctions deviate more and more from each other. Within our region $D_3$, the profiles of Orr–Sommerfeld eigenfunctions and Karhunen–Loève eigenfunctions are quite different, so that the structures described by the POD in the downstream part of our domain have to be considered truly nonlinear structures.

Having thus gained some confidence in the physical significance of the coherent structures as identified by POD, we now look at the structure of the flow within a selected region in more detail.

## 5. The coherent structures of the spike stages

The higher-order structures in region $D_2$ are now examined. This region is especially interesting not only because the Λ-vortex is most pronounced here (see figure 4), but also because the spike stages of transition occur within this region. These stages are named for the characteristic negative spikes in the time signals of the fluctuating $u$-velocity component $u'$ (Klebanoff, Tidstrom & Sargent 1962). Time signals typical for this stage are shown in figure 8 as obtained from the simulation by Rist *et al.* (1994). It should be noted that the occurrence of these spikes in the time traces of the $u'$-signal is highly localized and occurs in a relatively small region in the cross-stream $(y,z$-plane). Attempts were made by some to explain these spike signals as a consequence of a secondary instability of the instantaneous velocity profiles (Landahl 1972; Nishioka, Asai & Iida 1980), while others conjecture that the spikes result from the linear superposition of a system of waves that are synchronized in phase (Kachanov *et al.* 1985; Rist 1990). Based on our coherent structures point of view and using POD analysis, we will therefore attempt a closer look at the description

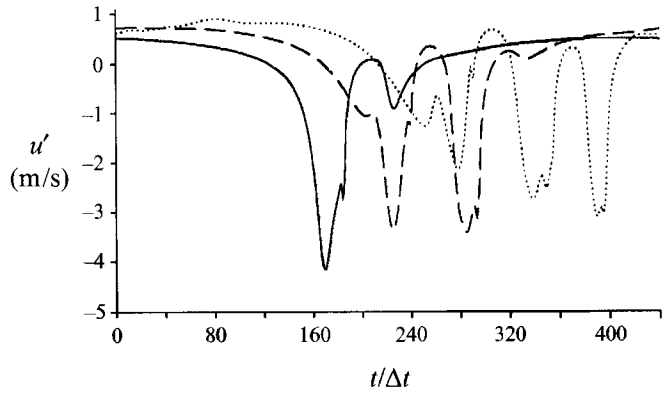


FIGURE 8. Signals of $u'$-component during the spike stages ($y = 3.11$ mm, $z = 0$). ————, one-spike-stage, $x = 430$ mm; — — —, two-spike-stage, $x = 440$ mm; ·····, three-spike-stage, $x = 450$ mm.

of the events occurring at the spike stages. That is, we would like to understand how the events of the spike stages can be depicted in terms of the behaviour of coherent structures.

The $u$- and $v$-isosurfaces of the coherent structures of second, third, and fourth order, together with the behaviour in time of the corresponding expansion coefficients $\zeta_j$, are shown in figures 9–11. The relative energies $\Lambda_j^\varsigma$ of each of the structures are noted. The first-order structure is shown in figure 5, and the time behaviour of its expansion coefficients appears in figure 2.

The $u$-velocity surface of the second-order structure (figure 9), contributing $\Lambda_2^\varsigma \approx 9.6\%$ to the energy of the fluctuating flow, is qualitatively similar to that of the first-order structure. It displays the same $\Lambda$-shape as the latter; however, the streamwise distance between consecutive structures, as well as the extension of the structure in the $x$-direction, is reduced by a factor of two. The $v$-velocity surface, however, is quite different from that of the first-order structure. It shows an evolution from a small arch to a pronounced horseshoe-like shape. For the third-order structure (figure 10, $\Lambda_3^\varsigma \approx 1.7\%$), the $u$-velocity surface and the $v$-isosurface are again similar to the corresponding shapes of the second-order structure, with the streamwise scales reduced by a factor of three in comparison to the first-order structure. From the behaviour of the expansion coefficients of the first three structures, it can be inferred that the energy of these structures,

$$e_j^\varsigma(t) = \tfrac{1}{2}(\zeta_{2j}^2(t)\lambda_{2j} + \zeta_{2j+1}^2(t)\lambda_{2j+1}), \tag{5.1}$$

is almost constant in time. Furthermore, by comparing the frequencies of the expansion coefficients and the streamwise 'wavelengths' of the first three structures, it can be seen that these structures are all travelling at the same speed in the streamwise direction. We also note that the increase in frequency of the higher-order expansion coefficients as 1 : 2 : 3 is the same as the one that was found in work by Rajaee & Karlsson (1990).

In contrast, the fourth-order structure, which contributes only 0.9% to the energy of the fluctuating flow, behaves completely differently. First of all, it can be seen especially well from the $v$-velocity surface that this structure is located almost entirely near the downstream end of the domain considered. It appears as if this structure

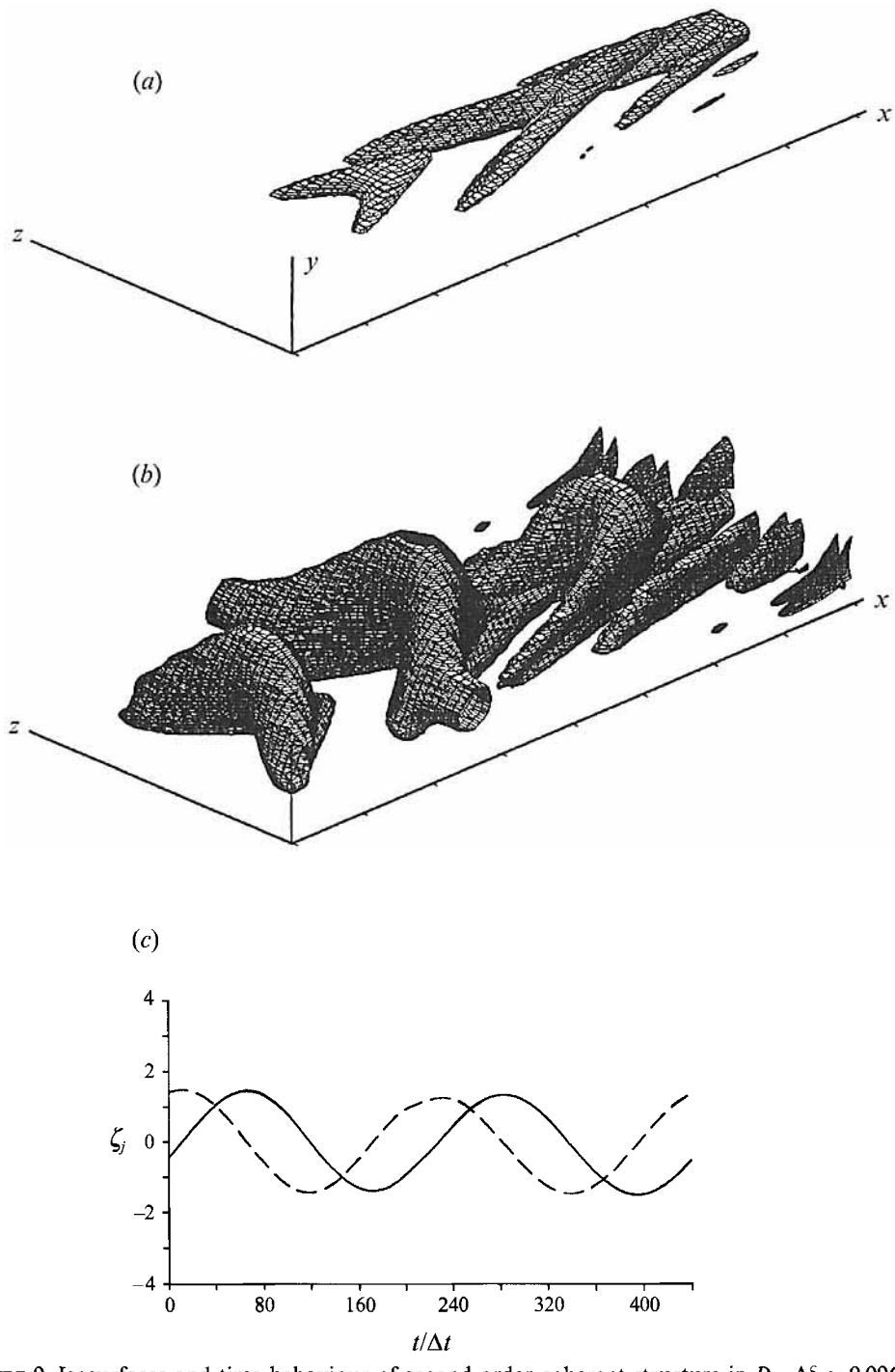


FIGURE 9. Isosurfaces and time behaviour of second-order coherent structure in $D_2$, $\Lambda_2^s \approx 0.096$, $t/\Delta t = 1$ (369 mm $\leqslant x \leqslant$ 438 mm).

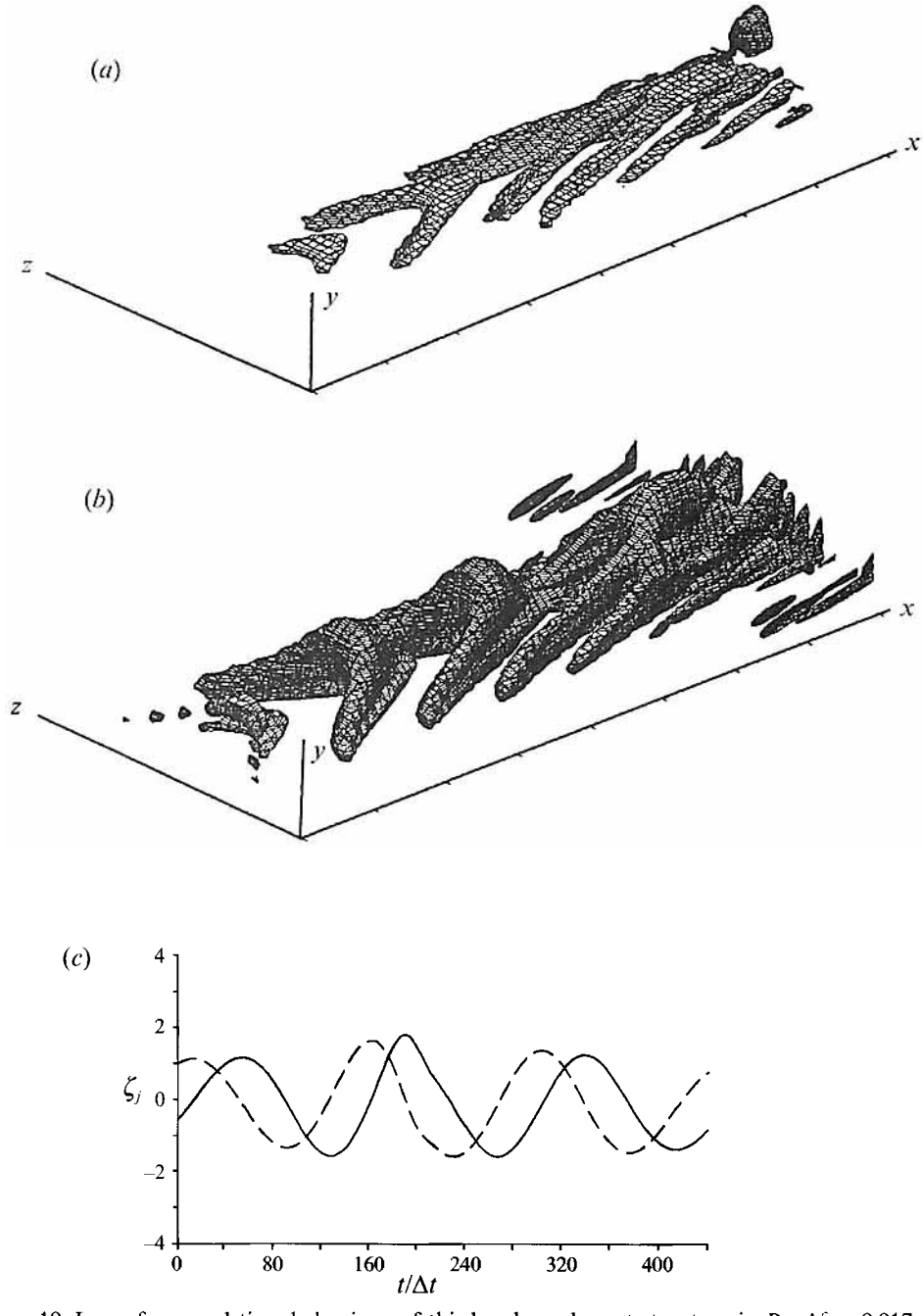


FIGURE 10. Isosurfaces and time behaviour of third-order coherent structure in $D_2$, $\Lambda_2^{\zeta} \approx 0.017$, $t/\Delta t = 1$ (369 mm $\leqslant x \leqslant$ 438 mm).

were still in the process of formation, and the shape of the isosurfaces of this structure is completely different from the ones of the lower-order structures. Furthermore, if we look at the behaviour of the expansion coefficients, it can be seen that the energy of this structure shows a steep increase at about $t/\Delta t = 160$ and falls back shortly afterwards. The energy increases by a factor of more than ten during this event. Thus, despite the low average contribution of the fourth-order structure to the energy of the flow, the influence of this structure is felt distinctly during the phase of high energy. This will become even more obvious when we look at the induced disturbance velocities (see below). The striking behaviour of the coefficients $\zeta_8$ and $\zeta_9$ shows obvious parallels to the spike signals of the $u$-velocity component, and indeed in the numerical simulation the spike stages of transition do occur within the last quarter of region $D_2$, which is where the fourth-order structure from figure 11 forms. We will therefore examine this structure in some more detail.

The contour surfaces of the $v$-velocity component of this structure are shown in figure 12 at four different instants in time during the phase of strongly increased energy. It can be seen how a structure that was initially tilted in the upstream direction is becoming more upright while it is growing in the wall-normal direction. At the last instance shown, the big 'blob' at the top of the structure appears to separate from the main structure. To show that this structure is actually connected to the spike signals, the $u$-velocity distribution of this structure is plotted in figure 13 at the moment of maximum energy in the cross-stream plane, $x = 435$ mm, that was indicated in figure 12. This distribution shows a negative peak just in the region where the spike signals are most pronounced. In order to assess the contribution of this structure to the spike of the $u'$-signal, the $u'$-signals that are induced by different coherent structures are plotted in figure 14 at a point of the cross-stream plane at $x = 435$ mm where the spike signals reach the maximum amplitude. The point chosen coincides with the one where the $u$-velocity distribution from figure 13 reaches its minimum. There it can be seen that, of all structures, the fourth one induces the largest negative $u'$-signal. While the passage of the first-order structure (the $\Lambda$-vortex) just leads to a smooth harmonic oscillation of $u'$, the action of the fourth-order structure actually generates the characteristic spikes.

Some more information on the properties of the fourth-order structure can be obtained by looking at the velocity vectors of its flow field within a cross-stream plane. In figure 15, the projection of the velocity vectors is plotted on the same cross-stream plane where the $u$-velocity distribution (figure 13) has been shown. It can be clearly seen that this structure induces a strong updraft of fluid away from the wall at the moment of maximum energy. Shortly afterwards, the structure generates a movement of fluid back towards the wall, which then is spreading in the spanwise direction in the near-wall region.

## 6. Discussion and conclusions

We will first point out some of the most important elements of the description of the flow phenomena at the spike stages that were obtained by investigating the coherent structures as identified by POD. We have seen that, indeed, the most energetic of the coherent structures of the flow is an object that clearly shows the typical shape of the well-known $\Lambda$-vortex. Thus we can say that, in contrast to previously expressed doubts (Sirovich 1989), the eigenfunctions of the POD are definitely capable of describing the spatially evolving structures in our case of a transitional flat-plate boundary layer. On the other hand, it should be noted that one major requirement to

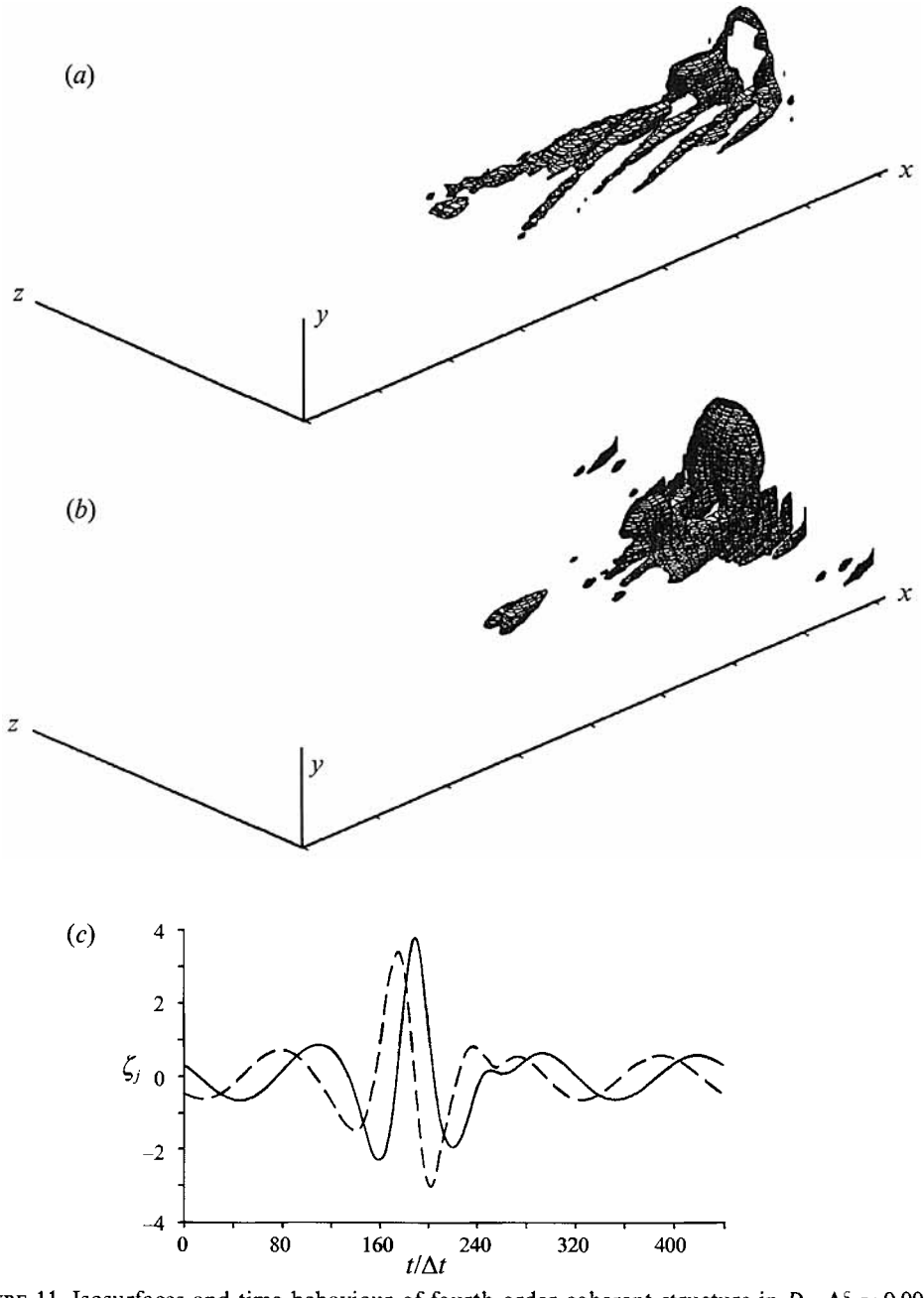


FIGURE 11. Isosurfaces and time behaviour of fourth-order coherent structure in $D_2$, $\Lambda_2^5 \approx 0.009$, $t/\Delta t = 1$ (369 mm $\leqslant x \leqslant$ 438 mm).

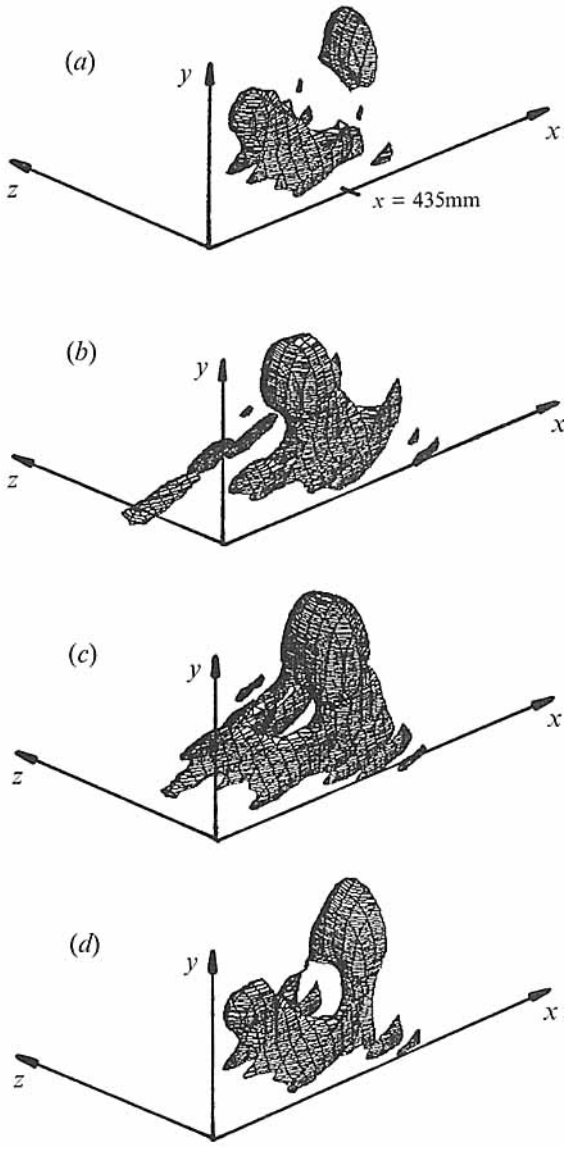


FIGURE 12. Isosurfaces $v = 0.05$ m/s of fourth-order coherent structure in $D_2$ during a spike.

reach this result was the availability of 'clean' numerically calculated flow fields that were symmetric along a coordinate that otherwise would have been a homogeneous direction. This symmetry of the flow fields leads to the coherent structures being aligned along the $x$-axis.

The structures determined by the POD method are similar to the ones that were found in experiments. Therefore, the decomposition of the flow into Karhunen–Loève eigenfunctions, defined by purely mathematical reasoning, organizes the phenomena occurring in the transitional boundary layer in a manner that is intuitively satisfying and seems to correspond to a decomposition a human observer could perform instinctively.

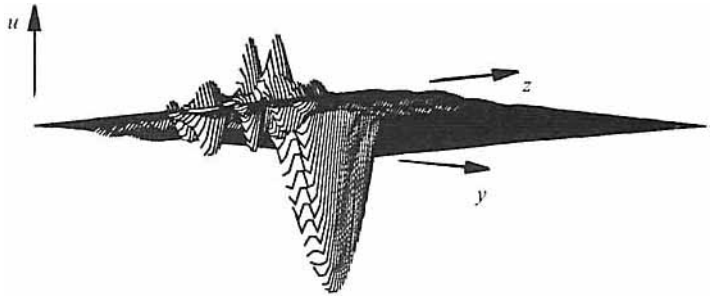


FIGURE 13. Distribution of $u$-component of fourth-order coherent structure within cross-stream plane $x = 435\,\text{mm}$ at $t/\Delta t = 180$.

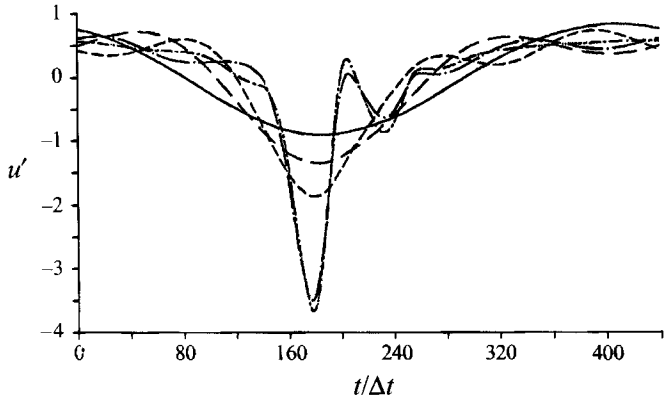


FIGURE 14. Superposition of signals of $u'$-component of coherent structures at $x = 435\,\text{mm}$, $y = 3.11\,\text{mm}$, $z = 0$. ————, first-order structure; — — —, up to second-order structure; – – – – –, up to third-order structure; —·—·—, up to fourth-order structure; —·—·—·—, up to fifth-order structure; ·····, up to sixth-order structure.

Our investigations of the events occurring at the spike stages have shown that the eigenfunctions of the POD offer the possibility of a compact description of complex flow phenomena. The functions $\varsigma_j$ that describe the velocity fields of the coherent structures not only give us 'typical' velocity distributions of coherent structures, but they contain complete information on the evolution of the structures. Thus, investigations of the $\varsigma_j$ are apt in addressing the criticism by Wallace & Hussain (1990) on current studies of coherent structures: '*It is not enough to know the most probable distributions of vorticity or velocity fluctuations. It is necessary to know how the patterns will evolve*' (p. S208, emphasis is ours). In particular, we have seen that the characteristic events of the spike stages can essentially be understood from the behaviour of one single coherent structure. This statement can be made although the action of the fourth-order structure alone does not allow a complete description of the phenomena characteristic of the spike stages. As in the case of the Λ-vortex, where two additional structures — the second and the third ones — described some finer details of a common pattern ('Λ-shape'), higher-order structures existed in the case of the 'spike-structure' that were not shown here. These add more details to the description of the spike events. However, owing to the fast convergence of the POD,

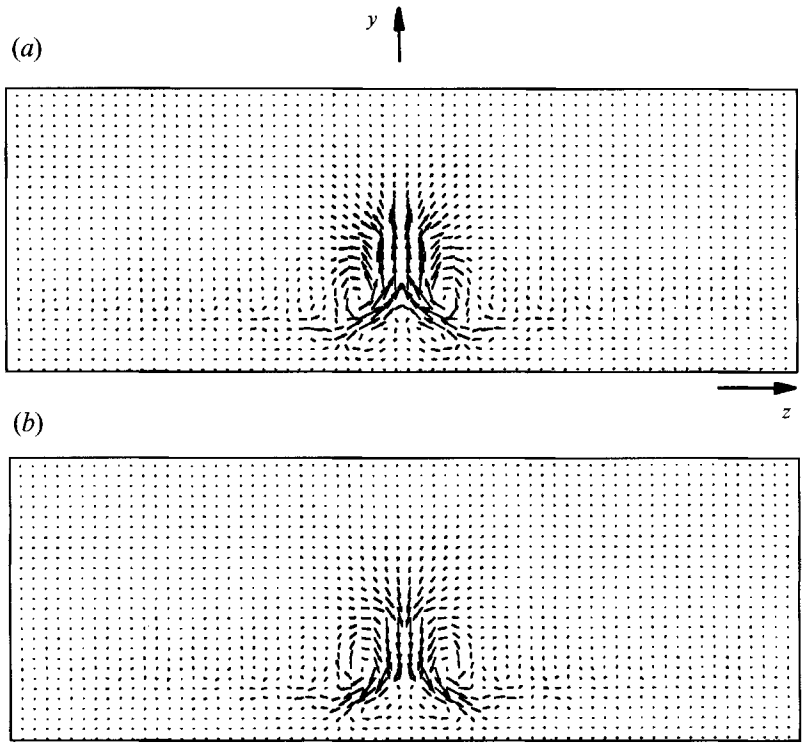


FIGURE 15. Velocity vectors of fourth-order coherent structure at cross-stream plane $x = 435$ mm.

these higher-order structures induce considerably smaller velocity fluctuations than the fourth-order structure (see figures 14 and 15).

We would also like to draw attention to the striking similarity of the phenomena occurring at the spike stages of a transitional boundary layer to the bursting event of fully turbulent boundary layers (Robinson 1991). The updraft of fluid shown in figure 15 (*a*) corresponds to the ejection phase of this bursting event and the movement of fluid shown in figure 15 (*b*) resembles the sweep phase of bursting. The detailed analogies between bursting and the phenomena of the spike stages as described here suggest corresponding similarities in the underlying mechanisms. Such analogies between transitional and fully turbulent boundary layers have been suggested before (for example by Blackwelder 1991). If they were real, our investigations could also shed some light on the bursting phenomenon of turbulent boundary layers. For instance, our results concerning the phenomena of the spike stages show that the 'ejection' of fluid during a spike cannot be interpreted as just an epiphenomenon of the passage of a $\Lambda$-vortex. Rather, this ejection of fluid, although probably being triggered by the passage of the $\Lambda$-vortex, seems to be an event *sui generis*. If this result can be extended to the bursting of turbulent boundary layers, models of bursting that describe this phenomenon as a simple side effect of the movement of a vortex (see Robinson 1991) would not be sufficient.

Finally, we note that, although the investigations reported here yielded additional insight into the phenomena occurring at the spike stages of transition, these were mainly on a phenomenological level describing basically the kinematics of coherent structures. Such explorations are not sufficient to clarify the causal interrelations of

the different phenomena. Referring back to the quotation of Wallace & Hussain above, we do not only want to know *how* the patterns evolve, we also want to know *why* they behave as they do. For instance, in the case of the fourth-order structure described above, the question arises as to how the extremely strong variations of the energy of this structure are created. We have therefore derived the detailed dynamical equations for the energy of the coherent structures. By looking at the energy flows within the system of coherent structures, we were able to reveal some of the mechanisms behind the behaviour of the coherent structures. The results of these investigations will be reported in a subsequent paper (Rempfer & Fasel 1994).

This research was supported by grants from the Studienstiftung des deutschen Volkes, Germany, and by the Office of Naval Research, USA.

## REFERENCES

AUBRY, N., GUYONNET, R. & LIMA, R. 1991 Spatiotemporal analysis of complex signals: theory and applications. *J. Statist. Phys.* **64**, 683–739.

AUBRY, N., GUYONNET, R. & LIMA, R. 1992 Spatio-temporal symmetries and bifurcations via bi-orthogonal decompositions. *J. Nonlin. Sci.* **2**, 183–215.

AUBRY, N., HOLMES, P., LUMLEY, J. L. & STONE, E. 1988 The dynamics of coherent structures in the wall region of a turbulent boundary layer. *J. Fluid Mech.* **192**, 115–173.

BAKEWELL, H. P. & LUMLEY, J. L. 1967 Viscous sublayer and adjacent wall region in turbulent pipe flow. *Phys. Fluids* A **10**, 1880–1889.

BALL, K. S., SIROVICH, L. & KEEFE, L. R. 1991 Dynamical eigenfunction decomposition of turbulent channel flow. *Intl J. Num. Meth. Fluids* **12**, 585–604.

BLACKWELDER, R. F. 1983 Analogies between transitional and turbulent boundary layers. *Phys. Fluids* A **26** (10), 2807–2815.

BREUER, K. S. & SIROVICH, L. 1991 The use of the Karhunen-Loève procedure for the calculation of linear eigenfunctions. *J. Comput. Phys.* **96**, 277–296.

DELVILLE, J., BELLIN, S. & BONNET, J. P. 1990 Use of the proper orthogonal decomposition in a plane turbulent mixing layer. In *Turbulence and Coherent Structures* (ed. O. Métais & M. Lesieur), pp. 75–90. Kluwer.

GLAUSER, M. N. & GEORGE, W. K. 1987 An orthogonal decomposition of the axisymmetric jet mixing layer utilizing cross-wire velocity measurements. In *Proc. 6th Symposium on Turbulent Shear Flows, Toulouse, France, September 7-9.*

GLEZER, A., KADIOGLU, Z. & PEARLSTEIN, A. J. 1989 Development of an extended proper orthogonal decomposition and its application to a time-periodically forced plane mixing layer. *Phys. Fluids* A **1**, 1363–1373.

HAMA, F. R. & NUTANT, J. 1963 Detailed flow-field observations in the transition process in a thick boundary layer. In *Proc., 1963 Heat Transfer and Fluid Mech. Inst.*, pp. 77–93. Stanford University Press.

KACHANOV, Y. S., KOZLOV, V. V., LEVCHENKO, V. Y. & RAMAZANOV, M. P. 1985 On the nature of K-breakdown of a laminar boundary-layer. New experimental data. In *Laminar-Turbulent Transition* (ed. V. V. Kozlov), pp. 61–73. Springer.

KIRBY, M., BORIS, J. & SIROVICH, L. 1990 An eigenfunction analysis of axisymmetric jet flow. *J. Comput. Phys.* **90**, 98–122.

KLEBANOFF, P. S., TIDSTROM, K. D. & SARGENT, L. M. 1962 The three-dimensional nature of boundary-layer instability. *J. Fluid Mech.* **12**, 1–34.

KLEISER, L. & ZANG, T. A. 1991 Numerical simulation of transition in wall-bounded shear flows. *Ann. Rev. Fluid Mech.* **23**, 495–537.

LANDAHL, M. T. 1972 Wave mechanics of breakdown. *J. Fluid Mech.* **56**, 775–802.

LOÈVE, M. 1955 *Probability Theory*. Van Nostrand.

LORENZ, E. N. 1963 Deterministic nonperiodic flow. *J. Atmos. Sci.* **20**, 130–141.

LUMLEY, J. L. 1967 The structure of inhomogeneous turbulent flows. In *Atmospheric Turbulence and Radio Wave Propagation* (ed. A. M. Yaglom & V. I. Tatarski), pp. 166–178. Nauka, Moskow.

LUMLEY, J. L. 1970 *Stochastic Tools in Turbulence*. Academic.

MOIN, P. & MOSER, R. D. 1989 Characteristic-eddy decomposition of turbulence in a channel. *J. Fluid Mech.* **200**, 471–509.

MONIN, A. S. & YAGLOM, A. M. 1973 *Statistical Fluid Mechanics*. MIT Press.

NISHIOKA, M., ASAI, M. & IIDA, S. 1980 An experimental investigation of the secondary instability. In *Laminar-Turbulent Transition*. (ed. R. Eppler & H. Fasel), pp. 113-126. Academic.

PARK, H. & SIROVICH, L. 1990 Turbulent thermal convection in a finite domain: Part II. Numerical results. *Phys. Fluids* A **2**, 1659–1668.

PERRY, A. E., LIM, T. T. & TEH, E. W. 1981 A visual study of turbulent spots. *J. Fluid Mech.* **104**, 387–405.

RAJAEE, M. & KARLSSON, S. K. F. 1990 Shear flow coherent structures via Karhunen-Loève expansion. *Phys. Fluids* A **2**, 2249–2251.

RAJAEE, M., KARLSSON, S. K. F. & SIROVICH, L. 1994 Low-dimensional description of free shear flow coherent structures and their dynamical behaviour. *J. Fluid Mech.* **258**, 1–29.

REMPFER, D. 1991 Kohärente Strukturen und Chaos beim laminar-turbulenten Grenzschichtumschlag. Dissertation, University of Stuttgart, Germany.

REMPFER, D. 1993 Low-dimensional models of a flat-plate boundary layer. In *Near-Wall Turbulent Flows* (ed. R. M. C. So, C. G. Speziale & B. E. Launder), pp. 63–72. Elsevier.

REMPFER, D. & FASEL, H. 1992 Dynamics of three-dimensional coherent structures in a flat-plate boundary layer. *J. Fluid Mech.* (submitted).

RIST, U. 1990 Numerische Untersuchung der räumlichen, dreidimensionalen Strömungsentwicklung beim Grenzschichtumschlag. Dissertation, University of Stuttgart, Germany

RIST, U., KLOKER, M. & FASEL, H. 1994 Numerical simulation of transition in a flat plate boundary layer. *J. Fluid Mech.* (submitted).

ROBINSON, S. K. 1991 Coherent motions in the turbulent boundary layer. *Ann. Rev. Fluid Mech.* **23**, 601–639.

SIROVICH, L. 1987 Turbulence and the dynamics of coherent structures. *Q. Appl. Maths* **45**, 561–590.

SIROVICH, L. 1989 Chaotic dynamics of coherent structures. *Physica* D **37**, 126–145.

SIROVICH, L., BALL, K. S. & HANDLER, K. H. 1991 Propagating structures in wall-bounded turbulent flows. *Theoret. Comput. Fluid Dyn.* **2**, 307–317.

SIROVICH, L., BALL, K. S. & KEEFE, L. R. 1990 Plane waves and structures in turbulent channel flow. *Phys. Fluids* A **2**, 2217–2226.

SIROVICH, L., KIRBY, M. & WINTER, M. 1990 An eigenfunction approach to large scale transitional structures in jet flow. *Phys. Fluids* A **2**, 127–136.

SIROVICH, L. & PARK, H. 1990 Turbulent thermal convection in a finite domain: Part I. theory. *Phys. Fluids* A **2**, 1649–1658.

WALLACE, J. M. & HUSSAIN, F. 1990 Coherent structures in turbulent shear flows. *Appl. Mech. Rev.* **43**, S203–S209.

WILLIAMS, D. R., FASEL, H. & HAMA, F. R. 1984 Experinmental determination of the three-dimensional vorticity field in the boundary-layer transition process. *J. Fluid Mech.* **149**, 179–203.

ZHOU, X. & SIROVICH, L. 1992 Coherence and chaos in a model of a turbulent boundary layer. *Phys. Fluids* A **4**, 2855–2874.